Journal of Solid Mechanics Vol. 12, No. 3 (2020) pp. 505-520
DOI: 10.22034/jsm.2019.581546.1365

Non-Linear Response of Torsional Buckling Piezoelectric Cylindrical Shell Reinforced with DWBNNTs Under Combination of Electro-Thermo-Mechanical Loadings in Elastic Foundation

M. Sarvandi [1], M.M. Najafizadeh [1] , H. Seyyedhasani [2,*]

[1]*Department of Mechanical Engineering, Arak Branch, Islamic Azad University, Arak, Iran*
[2]*School of Plant and Environmental Sciences, Virginia Polytechnic Institute and State University, Blacksburg, Virginia, USA*

Received 29 March 2020; accepted 24 May 2020

ABSTRACT

Nanocomposites provide new properties and exploit unique synergism between materials. Polyvinylidene fluoride (PVDF) is an ideal piezoelectric matrix applicable in nanocomposites in a broad range of industries from oil and gas to electronics and automotive. And boron nitride nanotubes (BNNTs) show high mechanical, electrical and chemical properties. In this paper, the critical torsional load of a composite tube made of PVDF reinforced with double-walled BNNTs is investigated, under a combination of electro-thermo-mechanical loading. First, a nanocomposite smart tube is modeled as an isotropic cylindrical shell in an elastic foundation. Next, employing the classical shell theory, strain-displacement equations are derived so loads and moments are obtained. Then, the total energy equation is determined, consisting of strain energy of shell, energy due to external work, and energy due to elastic foundation. Additionally, equilibrium equations are derived in cylindrical coordinates as triply orthogonal, utilizing Euler equations; subsequently, stability equations are developed through the equivalent method in adjacent points. The developed equations are solved using the wave technique to achieve critical torsional torque. Results indicated that critical torsional buckling load occurred in axial half-wave number m = 24 and circumferential wave number n = 1, for the investigated cylindrical shell. The results also showed that with the increase in the length-to-radius ratio and in the radius-to-shell thickness ratio, the critical torsional buckling load increased and decreased, respectively. Lastly, results are compared in various states through a numerical method. Moreover, stability equations are validated via comparison with the shell and sheet equations in the literature.

Keywords: Torsional buckling; Piezoelectric; Electro-thermo-mechanic; Elastic foundation; Cylindrical shell.

1 INTRODUCTION

OVER the last decade, the developed nanocomposites have been immensely receiving attention. This comes from their unique properties and the synergy of incorporated materials. Polyvinylidene fluoride (PVDF) is

*Corresponding author. Tel.: +1 859 536-8233.
E-mail address: seyyedhasani12@vt.edu (H. Seyyedhasani).

considered among the best piezoelectric matrices. It has a number of properties that make it an ideal matrix: 1) flexible in thermoplastic conversion techniques, 2) excellent dimensional stability, 3) resistant against abrasion and corrosion, and 4) preserving mechanical properties at high temperatures. Thus, they are being increasingly applied in various industries. Additionally, boron nitride nanotubes (BNNTs) have high resistance against oxidation. This composite can be used as a matrix reinforcer that outperforms the widely used nanoreinforcers like carbon nanotubes (CNTs) [1,2] Studying cylindrical shells made of functionally graded material (FGM) had been an area of interest to many researchers. Sofiyev [3] investigated the buckling of FG cylindrical shells, subjected to axial loads and hydrostatic pressure. Miraliyari, Najafizadeh [4] analyzed the buckling of FG cylindrical shells with various lengths. They determined the equilibrium and stability equations using the total potential energy and Euler equations. Their results demonstrated long cylindrical shells have zero axial strain, under thermal and mechanical loads. Additionally, the critical pressure increased with either the increase of thickness to radius ratio, or the increase of length to radius ratio. According to Bagherizadeh, Kiani [5] the critical buckling load of FG cylindrical shells increases in elastic medium. The critical buckling loads also increase with the increase of the shell thickness and decrease of the inhomogeneity Najafizadeh, Hasani [6]. Sheng and Wang [7] worked on thermoelastic vibration and buckling characteristics of the FGM cylindrical shells. Using the Hamilton's principle, the Maxwell equation, and First-order Shear Deformation Theory (FSDT), the cylindrical shell made of various material was studied, in terms of direct piezoelectric, converse piezoelectric, thermoelastic vibration, and buckling characteristics. Their results showed fundamental frequency and axial critical load in cylindrical shells made of BaTiO3/PZT 4 is higher than those made of BaTiO3/PZT 5A and BaTiO3/PVDF. Additionally as the temperature differences between the inside and outside surfaces of the cell increases, the fundamental frequency decreases. Shen, Yang [8] studied the post buckling response of a FG cylindrical shell of finite length embedded in a large outer elastic medium and subjected to internal pressure in thermal environments. The post buckling analysis was based on a higher-order shear deformation theory (HSDT) with von Kármán-Donnell-type of kinematic nonlinearity. The results showed that the unilateral constraint has a significant effect on the post buckling response of shells when the foundation stiffness was sufficiently large. As it is evident, there are a lot of research need with regard to cylindrical shells made of pizoelectic materials. Most of buckling analysis on cylindrical shells in the literature had aimed at linear responses. Najafizadeh and Khazaeinejad [9] studied the buckling analysis of a nonhomogeneous cylindrical shell under torsion. They derived stability equations based on the FSDT and examined the validity of the analysis through comparing their results with those in the literature. The results show that the critical torsional load changed linearly when non-homogeneous parameters of the material changed, and the amount of the critical torsional load decreased when the thickness increased. Hassani, Jafari [10] investigated the transient heat transfer performed by a fluid power system through finite element method (FEM). They converted all the components of the system into a homogeneous one (30-*mm* long steel pipe) to calculate temperature increase due to the energy losses. Their results demonstrated after five hours working in field conditions the temperature of the inside surface of the modeled pipe will be 70°C, as the hottest area. The buckling analysis of piezoelasticity cylindrical shells by Arani , Amir [11] has shown that direct and reverse voltages, on the shells, decrease and increase the nonlocal buckling load, respectively. Additionally, the nonlocal critical buckling load, $(m,n) = (78,0)$, was less than the local critical buckling load. To determine linear buckling responses of conical composite shells, Shadmehri, Hoa [12] put forward a semi-analytical technique. They represented the governing equilibrium equations using the minimum total potential energy rule, and solved the equations using the Ritz method. Arani, Barzoki [13] studied PZT-5 piezoelectric hollow cylinders. They represented creep strains for displacement, using a differential equation, and demonstrated the dynamic increase of electric potentials. Therefore, studying the non-linear response of piezoelectric cylinder shell is a potential research area. The critical buckling loads on cylindrical shells have been characterized according to the power law index: Khazaeinejad, Najafizadeh [14] studied the stability of cylindrical shells made of functionally graded material (FGM), which were under external pressure and axial compression loads. To determine the critical buckling loads, they employed the FSDT. Hence, characterizing the critical torsional buckling loads according to axial half-wave number and circumferential wave number is a contribution towards the optimal design of smart composites. Thermal changes is one of the main drivers in designed devices given the effect of materials and vibrational responses. In addition, Zargaripoor, Daneshmehr [15] studied the free vibration in FGM nanoplates using third-order shear deformation plate theory. Additionally, Moradi, Yaghootian [16] showed the vibration response of FG circular and annular Nanoplate is largely dependent upon size-dependent parameter; and temperature changes highly affected their mechanical behavior. This is also true about regular nanoplates [17, 18]. Shen and Zhang [19] studied torsional buckling and post buckling of CNTs, under torsion in thermal ambiance, using the HSDT. Their results demonstrated, for both single-walled and double-walled CNTs, the dependency in size and temperature of material properties is drastically effective on the torsional buckling and post buckling behavior. Mantari, Oktem [20] developed a theory for shear deformation of composite plates, using the principle of virtual work. The theory deals

with the distribution of the shear strains on the plate boundary. Hassani, Jafari [21] investigated the contact and fatigue analysis, using FEM. They estimated the critical points susceptible to the crack growth via the fully reverse loading. However, considering electro-thermo-mechanical medium results in more realistic studies. Arani, Kolahchi [22] studied the effect of material in-homogeneity on rotary shafts, in an electro-thermo-mechanical medium. The equations were derived according to HSDT. Their investigation on various boundary conditions showed the optimal design of the material in-homogeneity factor is among the influential factors. Arani, Abdollahian [23] investigated electro-thermo-torsional buckling of an embedded armchair double-walled boron nitride nanotubes (DWBNNTs). They showed the piezoelectricity reduces the critical buckling load, using nonlocal elasticity and piezoelectricity theory. The volume fraction of nanotube is a main factor in determining the critical load and stability of a system. Arani, Shajari [24] investigated nonlinear vibration and stability of a smart composite micro-tube made of PVDF reinforced by BNNTs embedded in an elastic medium under electro-thermal load. The smart micro-tube was modeled as a thin shell based on the nonlinear Donnell's shell theory. It has also been found that the stability of the system was strongly dependent on the imposed electric potential and the volume percent of BNNTs reinforcement. Additionally, their results indicated that increasing mean flow velocity considerably increased the nonlinearity effects so that small scale and temperature change effects became negligible. Ansari, Rouhi [25] employed FEM to achieve thermal conductivity coefficients of CNTs reinforced polypropylene. They showed that the polypropylene reinforced by the regular distribution of nanotubes experience the largest thermal conductivity coefficients; additionally, larger volume percentages of CNTs generate larger thermal conductivity coefficients. Many studies have been conducted on the effect of length to radius ratio on the torsional buckling of the piezoelectric cylindrical shell reinforced by BNNTs. Barzoko, Arani [26] investigated electro-thermo-mechanical torsional buckling of a piezoelectric polymeric cylindrical shell reinforced by DWBNNTs with an elastic core, using Donnell linear theory and energy method. Their results showed that in low values of length to radius ratio (L/R), the critical buckling load is high and reduces sharply down to $L/R = 1.5$; also the shell buckling strength increased substantially as harder foam cores are employed. Kargarnovin and Shahsanami [27] showed: 1) the critical buckling load is less in comparison to isotropic cylindrical shells; 2) reinforcing cylindrical shells with FGM fibers reduces this metric compared to metal; 3) an inverse relationship between the critical buckling load and length-to-radius ratio in cylindrical shells. In addition, Barzoki, Arani [28] investigated nonlinear buckling of a cylindrical shell made of PVDF, in an electro-thermo-mechanical medium. They used the Hamilton's principle and the FSDT to determine the equilibrium and displacement equations. Additionally, the harmonic differential quadrature method was used to determine the critical buckling load under the existence of electro-mechanical boundary conditions surrounding the cylindrical shell. They concluded that by considering piezoelectric effect the buckling load happened to be critical. And the increase of L/R ratios doesn't affect the minimum critical buckling load; however, the increase affects the location of the critical load to be farther along the shell. To the best of the authors knowledge, no study has considered the effect of radius to thickness on the torsional buckling of such smart composites. Hence, such an investigation appears to be a necessity. As the literature study suggested, even though a significant amount of research has been conducted on smart composites, there are still significant gaps towards the optimal design of next generation of Nano devices. Motivated by these considerations, in order to improve the optimum design of smart composites, in this work we aimed at studying non-linear analysis for the torsional buckling of a composite tube made of PVDF reinforced by DWBNNTs under combined electro-thermo-mechanical loadings in order to achieve critical torsional torque.

This study makes two contributions to the literature: 1) characterizes the critical torsional buckling loads based on wave analysis including axis half-wave number and circumferential wave number, in an elastic medium including Winkler and Pasternak foundation; 2) studies the physical characterization of the cylinder shell and volume percent of the embedded nanotubes on the critical torsional buckling load. The remaining of this paper is organized as follows: Section 2.1 presents the displacement field for a cylindrical shell model. In Section 2.2, the simplified stress-strain relations are presented, utilizing Donnell theory; subsequently, the relations between force and moments with internal stress are presented in Section 2.4. Then in Section 2.5, equilibrium equations are derived utilizing Euler equations; following that, in Section 2.6, stability equations are developed through equivalent method in adjacent point. And in Section 2.7, the developed equations are solved using the wave technique in order to achieve critical torsional torque, and represent the deformation of the buckling in cylindrical shells under torsional loads is expressed as a function of axial and circumferential waves. The Section 3, presents the results taking into account the influences of electric and thermal fields, elastic medium and small scale parameter on the electro-thermo-mechanical buckling behavior of DWBNNTs. Finally, the work is concluded in Section 4.

2 MATERIALS AND METHODS

2.1 Strain-deformation equations

The schematic diagram of a cylindrical shell made of PVDF reinforced with DWBNNTs and embedded in an elastic foundation is shown in Fig.1.The geometrical parameters of the cylindrical shell are indicated by length *L*, radius *R*, and thickness *h*. The diagram also shows the arbitrary coordination system. By utilizing classical shell theory, the displacement field for a cylindrical shell model is as following [7,26,28]:

$$u(x,\theta,z) = u_o(x,\theta) - z w_{o,x}(x,\theta) \tag{1}$$

$$v(x,\theta,z) = v_o(x,\theta) - z w_{o,\theta}(x,\theta) \tag{2}$$

$$w(x,\theta,z) = w_o(x,\theta) \tag{3}$$

where u, v and w denote displacements of an arbitrary point of shell in axial, circumferential and radial directions, respectively; u_0, v_0 and w_0 indicate point displacements on the middle plane of the shell, and z is the distance from an arbitrary point of the shell to the middle plane.

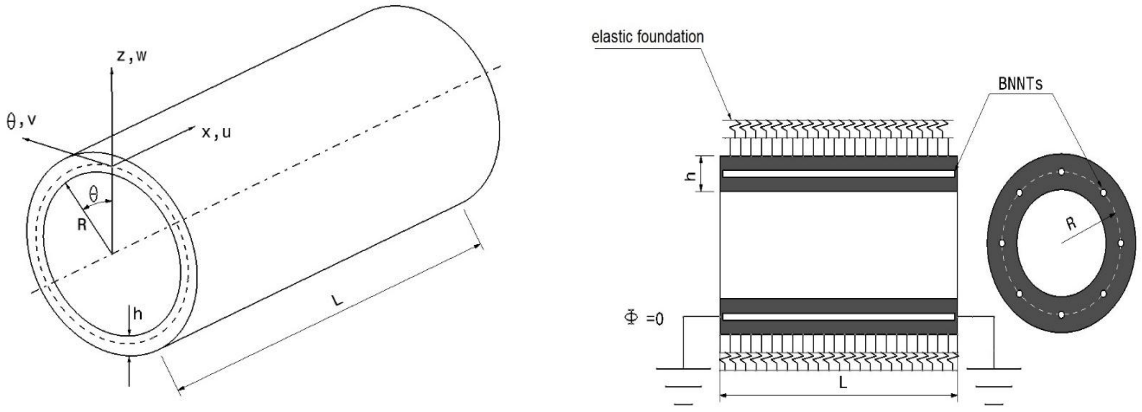

Fig.1
Cylindrical shell made of PVDF, reinforced with DWBNNTs embedded in an elastic foundation.

In addition, strain terms follow as [28]:

$$\begin{Bmatrix} \varepsilon_x \\ \varepsilon_\theta \\ \gamma_{x\theta} \end{Bmatrix} = \begin{pmatrix} \dfrac{\partial u_0}{\partial x} \\ \dfrac{\partial v_0}{R\partial\theta} + \dfrac{w_0}{R} \\ \dfrac{\partial u_0}{R\partial\theta} + \dfrac{\partial v_0}{\partial x} \end{pmatrix} + \begin{pmatrix} \dfrac{1}{2}\left(\dfrac{\partial w_0}{\partial x}\right)^2 \\ \dfrac{1}{2}\left(\dfrac{\partial w_0}{R\partial\theta}\right)^2 \\ \dfrac{\partial w_0}{\partial x}\dfrac{\partial w_0}{R\partial\theta} \end{pmatrix} - z \begin{pmatrix} \dfrac{\partial^2 w_0}{\partial x^2} \\ \dfrac{\partial^2 w_0}{R^2\partial\theta^2} \\ 2\dfrac{\partial^2 w_0}{R\partial x\,\partial\theta} \end{pmatrix} = \tag{4}$$

$$\begin{Bmatrix} \varepsilon_{xm} \\ \varepsilon_{\theta m} \\ \gamma_{x\theta m} \end{Bmatrix}_L + \begin{Bmatrix} \varepsilon_{xm} \\ \varepsilon_{\theta m} \\ \gamma_{x\theta m} \end{Bmatrix}_{NL} + z \begin{Bmatrix} k_x \\ k_\theta \\ k_{x\theta} \end{Bmatrix} = \varepsilon_i^0 + z k_i \qquad i = x,\theta,x\theta$$

$$\begin{Bmatrix} k_x \\ k_\theta \\ k_{x\theta} \end{Bmatrix} = -\begin{Bmatrix} \dfrac{\partial^2 w_0}{\partial x^2} \\ \dfrac{\partial^2 w_0}{R^2 \partial \theta^2} \\ 2\dfrac{\partial^2 w_0}{R\,\partial x\,\partial \theta} \end{Bmatrix} \tag{5}$$

where $\gamma_{x\theta}$, ε_x, and ε_θ are mechanical strain parameters for an arbitrary point of shell, which depends on strains of the middle plane as $\varepsilon_{x,0}$, $\varepsilon_{\theta,0}$, and $\varepsilon_{x\theta,0}$, as well as bending and torsion of the middle plane as k_x, k_θ, and $k_{x\theta}$.

2.2 Stress-strain equations

Applying an electric field to piezoelectric material produces a strain proportional to the mechanical field strength, which is a reversible process. The constitutive equation is arbitrarily combined for matrix of stresses σ and strains ε matrix on the mechanical side, as well as matrix of flux density (D) and matrix of field strength (E) on the electrostatic side as bellow [26]:

$$\begin{Bmatrix} \sigma_x \\ \sigma_\theta \\ \sigma_z \\ \tau_{\theta z} \\ \tau_{xz} \\ \tau_{x\theta} \end{Bmatrix} = \begin{bmatrix} C_{11} & C_{12} & C_{13} & 0 & 0 & 0 \\ C_{21} & C_{22} & C_{23} & 0 & 0 & 0 \\ C_{31} & C_{32} & C_{33} & 0 & 0 & 0 \\ 0 & 0 & 0 & C_{44} & 0 & 0 \\ 0 & 0 & 0 & 0 & C_{55} & 0 \\ 0 & 0 & 0 & 0 & 0 & C_{66} \end{bmatrix} \left(\begin{Bmatrix} \varepsilon_x \\ \varepsilon_\theta \\ \varepsilon_z \\ \gamma_{\theta z} \\ \gamma_{xz} \\ \gamma_{x\theta} \end{Bmatrix} - \begin{Bmatrix} \alpha_x \\ \alpha_\theta \\ \alpha_z \\ 0 \\ 0 \\ 0 \end{Bmatrix} \Delta T \right) - \begin{bmatrix} 0 & 0 & e_{31} \\ 0 & 0 & e_{32} \\ 0 & 0 & e_{33} \\ 0 & e_{42} & 0 \\ e_{51} & 0 & 0 \\ 0 & 0 & 0 \end{bmatrix} \begin{Bmatrix} E_x \\ E_\theta \\ E_z \end{Bmatrix} \tag{6}$$

$$\begin{Bmatrix} D_x \\ D_\theta \\ D_z \end{Bmatrix} = \begin{bmatrix} 0 & 0 & 0 & 0 & e_{51} & 0 \\ 0 & 0 & 0 & e_{42} & 0 & 0 \\ e_{31} & e_{32} & e_{33} & 0 & 0 & 0 \end{bmatrix} \left(\begin{Bmatrix} \varepsilon_x \\ \varepsilon_\theta \\ \varepsilon_z \\ \gamma_{\theta z} \\ \gamma_{xz} \\ \gamma_{x\theta} \end{Bmatrix} - \begin{Bmatrix} \alpha_x \\ \alpha_\theta \\ \alpha_z \\ 0 \\ 0 \\ 0 \end{Bmatrix} \Delta T \right) - \begin{bmatrix} \in_{11} & 0 & 0 \\ 0 & \in_{22} & 0 \\ 0 & 0 & \in_{33} \end{bmatrix} \begin{Bmatrix} E_x \\ E_\theta \\ E_z \end{Bmatrix} \tag{7}$$

Lastly, stress and strain relations are simplified utilizing the Donnell theory for the composite shell, as below:

$$\begin{Bmatrix} \sigma_x \\ \sigma_\theta \\ \tau_{x\theta} \\ D_x \end{Bmatrix} = \begin{bmatrix} C_{11} & C_{12} & 0 & -e_{31} \\ C_{12} & C_{22} & 0 & -e_{32} \\ 0 & 0 & C_{66} & 0 \\ e_{31} & e_{32} & 0 & \in_{11} \end{bmatrix} \begin{Bmatrix} \varepsilon_x - \alpha_x \Delta T \\ \varepsilon_\theta - \alpha_\theta \Delta T \\ \gamma_{x\theta} \\ E_x \end{Bmatrix} \tag{8}$$

where $C_{ij}, e_{ij}, \varepsilon_{ii} (i, j = 1,...,6), \alpha_k (k = x, \theta, z)$, ΔT, and E_{xx} are elastic constants, piezoelectric constants, dielectric constants, thermal expansion coefficient, thermal gradient, and electric field, respectively. The electric field is defined as a function of electric potential, ϕ_{xx}, as below [28].

$$E_k = -\nabla \phi \tag{9}$$

BNNTs have two structures of Zigzag and Armchair ones. Zigzag tubes have a piezoelectric response lengthwise for one-axial stress, while armchair tubes have an electrical linear torque which is two-polar and dependent on

torsion. Hence, armchair structure of BNNTs has been employed in order to investigate the torsional resistance behavior of smart composites for this study. Moreover, DWBNNTs were preferred to one-walled BNNTs due to their high level strength and stability in applications with mechanical resistance requisites, and also their high amount of hardness and thermal conductivity.

2.3 Micro-electromechanically model

Aimed at modeling, PVDF and DWBNNTs were taken into account as the main matrix and reinforced materials, respectively. In addition, the shell of polymeric piezoelectric fiber reinforced composites (PPFRC) with their constituents assumed to be orthotropic and homogeneous with respect to their major axes. To evaluate the effective properties of a PPFRC unit cell, Tan and Tong [29] approach was adopted in which they use representative volume element based on micromechanical models. Their approach utilizes RVE based on micromechanical models, first the properties of the required strips made from piezoelectric fiber reinforced composite (PFRC) are obtained using the appropriate '*X* model' in association with the '*Y* model' (or vice-versa). Then, the properties of a PPFRC unit cell are calculated using '*XY* (or *YX*) rectangle model' (Fig.2). The closed-form formula used in '*X* model' (or '*Y* model') expressing the mechanical, thermal and electrical properties of the composite as explained in Eq. (6) and Eq. (7) above are [29]:

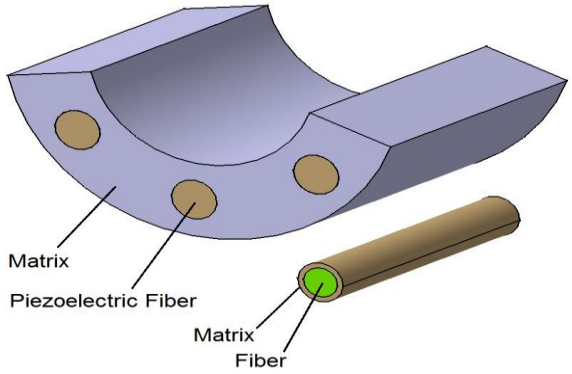

Fig.2
A schematic of RVE and DBNNTs reinforced composite.

where coefficients C_{ij} $(i,j = 1,2,3,4,5)$ of matrix (6) are given as below:

$$C_{11}=\frac{C_{11}^{r}C_{11}^{m}}{\rho C_{11}^{m}+(1-\rho)C_{11}^{r}},\qquad C_{12}=C_{11}[\frac{\rho C_{12}^{r}}{C_{11}^{r}}+\frac{(1-\rho)C_{12}^{m}}{C_{11}^{m}}],\qquad C_{13}=C_{11}[\frac{\rho C_{13}^{r}}{C_{11}^{r}}+\frac{(1-\rho)C_{13}^{m}}{C_{11}^{m}}]$$

$$C_{22}=\rho C_{22}^{r}+(1-\rho)C_{22}^{m}+\frac{C_{12}^{2}}{C_{11}}-\frac{\rho(C_{12}^{r})^{2}}{C_{11}^{r}}-\frac{(1-\rho)(C_{12}^{m})^{2}}{C_{11}^{m}},\qquad C_{44}=\rho C_{44}^{r}+(1-\rho)C_{44}^{m},\qquad C_{55}=\frac{A}{B^{2}+AC},$$

$$C_{23}=\rho C_{23}^{r}+(1-\rho)C_{23}^{m}+\frac{C_{12}C_{13}}{C_{11}}-\frac{\rho C_{12}^{r}C_{13}^{r}}{C_{11}^{r}}-\frac{(1-\rho)C_{12}^{m}C_{13}^{m}}{C_{11}^{m}},\qquad C_{66}=\frac{C_{66}^{r}C_{66}^{m}}{\rho C_{66}^{m}+(1-\rho)C_{66}^{r}}$$

$$e_{31}=C_{11}[\frac{\rho e_{31}^{r}}{C_{11}^{r}}+\frac{(1-\rho)e_{31}^{m}}{C_{11}^{m}}],\qquad e_{32}=\rho e_{32}^{r}+(1-\rho)e_{32}^{m}+\frac{C_{12}e_{31}}{C_{11}}-\frac{\rho C_{12}^{r}e_{31}^{r}}{C_{11}^{r}}-\frac{(1-\rho)C_{12}^{m}e_{31}^{m}}{C_{11}^{m}}$$

$$e_{33}=\rho e_{33}^{r}+(1-\rho)e_{33}^{m}+\frac{C_{13}e_{31}}{C_{11}}-\frac{\rho C_{13}^{r}e_{31}^{r}}{C_{11}^{r}}-\frac{(1-\rho)C_{13}^{m}e_{31}^{m}}{C_{11}^{m}},\qquad e_{24}=\rho e_{24}^{r}+(1-\rho)e_{24}^{m},\quad e_{15}=\frac{B}{B^{2}+AC}$$

$$\in_{11}=\frac{C}{B^{2}+AC}\qquad \in_{22}=\rho\in_{22}^{r}+(1-\rho)\in_{22}^{m}\qquad \in_{33}=\rho\in_{33}^{r}+(1-\rho)\in_{33}^{m}-\frac{(e_{31})^{2}}{C_{11}}+\frac{\rho(e_{31}^{r})^{2}}{C_{11}^{r}}+\frac{(1-\rho)(e_{31}^{m})^{2}}{C_{11}^{m}},$$

$$A=\frac{\rho C_{55}^{r}}{(e_{15}^{r})^{2}+C_{55}^{r}\in_{11}^{r}}+\frac{(1-\rho)C_{55}^{m}}{(e_{15}^{m})^{2}+C_{55}^{m}\in_{11}^{m}}\qquad B=\frac{\rho e_{15}^{r}}{(e_{15}^{r})^{2}+C_{55}^{r}\in_{11}^{r}}+\frac{(1-\rho)e_{15}^{m}}{(e_{15}^{m})^{2}+C_{55}^{m}\in_{11}^{m}}$$

$$C=\frac{\rho\in_{11}^{r}}{(e_{15}^{r})^{2}+C_{55}^{r}\in_{11}^{r}}+\frac{(1-\rho)\in_{11}^{m}}{(e_{15}^{m})^{2}+C_{55}^{m}\in_{11}^{m}}$$

2.4 Force and moment equations

Relation between forces and moments with internal stresses is specified as below [23]:

$$(N_i, M_i) = \int_{-\frac{h}{2}}^{\frac{h}{2}} \sigma_i (1, z)\mathrm{d}z \qquad i = x, \theta, x\theta \tag{10}$$

Substituting stress and strain relations from the Eqs. (8) in the Eq. (10), force and moment equations in terms of strains are obtained as followings:

$$\begin{Bmatrix} N_x \\ M_x \\ N_\theta \\ M_\theta \\ N_{x\theta} \\ M_{x\theta} \\ F_x \end{Bmatrix} = \begin{bmatrix} A_{11} & A_{12} & A_{13} & A_{14} & 0 & 0 & A_{17} \\ A_{21} & A_{22} & A_{23} & A_{24} & 0 & 0 & A_{27} \\ A_{31} & A_{32} & A_{33} & A_{34} & 0 & 0 & A_{37} \\ A_{41} & A_{42} & A_{43} & A_{44} & 0 & 0 & A_{47} \\ 0 & 0 & 0 & 0 & A_{55} & A_{56} & 0 \\ 0 & 0 & 0 & 0 & A_{65} & A_{66} & 0 \\ A_{71} & A_{72} & A_{73} & A_{74} & 0 & 0 & A_{77} \end{bmatrix} \begin{Bmatrix} \varepsilon_x^0 - \alpha_x \Delta T \\ k_x \\ \varepsilon_\theta^0 - \alpha_\theta \Delta T \\ k_\theta \\ \gamma_{x\theta}^0 \\ k_{x\theta} \\ E_x \end{Bmatrix} \tag{11}$$

where coefficients A_{ij} (i,j = 1,2,3,4,5,6,7) are given as below

$$A_{11} = \int_{-h/2}^{h/2} C_{11}\mathrm{d}z = C_{11}h \qquad A_{12} = A_{21} = \int_{-h/2}^{h/2} C_{11} z\mathrm{d}z = 0 \qquad A_{23} = A_{32} = \int_{-h/2}^{h/2} C_{12} z\mathrm{d}z = 0$$

$$A_{24} = A_{42} = \int_{-h/2}^{h/2} C_{12} z^2\mathrm{d}z = \frac{C_{12}h}{12} \qquad A_{13} = A_{31} = \int_{-h/2}^{h/2} C_{22}\mathrm{d}z = C_{12}h$$

$$A_{27} = A_{72} = \int_{-h/2}^{h/2} e_{31} z\mathrm{d}z = 0 \qquad A_{14} = A_{41} = \int_{-h/2}^{h/2} C_{12} z\mathrm{d}z = 0 \qquad A_{33} = \int_{-h/2}^{h/2} C_{22}\mathrm{d}z = C_{22}h$$

$$A_{17} = A_{71} = \int_{-h/2}^{h/2} e_{31}\mathrm{d}z = e_{31}h \qquad A_{34} = A_{43} = \int_{-h/2}^{h/2} C_{22} z\mathrm{d}z = 0 \qquad A_{22} = \int_{-h/2}^{h/2} C_{11} z^2\mathrm{d}z = \frac{C_{11}h}{12}$$

$$A_{37} = A_{73} = \int_{-h/2}^{h/2} e_{32}\mathrm{d}z = e_{32}h \qquad A_{44} = \int_{-h/2}^{h/2} C_{22} z^2\mathrm{d}z = \frac{C_{22}h}{12} \qquad A_{56} = A_{65} = \int_{-h/2}^{h/2} C_{66} z\mathrm{d}z = 0$$

$$A_{47} = A_{74} = \int_{-h/2}^{h/2} e_{32} z\mathrm{d}z = 0 \qquad A_{66} = \int_{-h/2}^{h/2} C_{66} z^2\mathrm{d}z = \frac{C_{66}h}{12} \qquad A_{55} = \int_{-h/2}^{h/2} C_{66}\mathrm{d}z = C_{66}h$$

$$A_{77} = \int_{-h/2}^{h/2} \in_{11} \mathrm{d}z = \in_{11} h$$

2.5 Equilibrium equations

The potential energy of the cylindrical shell is defined as [26]:

$$U = \frac{1}{2}\int_V (\sigma_x \varepsilon_x + \sigma_\theta \varepsilon_\theta + \sigma_{x\theta}\gamma_{x\theta} - D_x E_x)\mathrm{d}V \tag{12}$$

and potential energy attributed to work of torsional moment, applied on shell is stated as following:

$$\Omega = -\tau h \int_A (u_{0,\theta} + v_{0,x})\mathrm{d}A \tag{13}$$

where τ denotes torsional moment applied on shell and h is shell thickness. In addition, work due to the elastic foundation is defined as [5]:

$$W = \frac{1}{2}\int_A [k_w w_0^2 + k_g (w_{0,x}^2 + \frac{1}{R^2} w_{0,\theta}^2)]\mathrm{d}A \tag{14}$$

where k_g and k_w are Pasternak and Winkler parameters of elastic foundation, respectively. Total potential energy is derived as below:

$$\begin{aligned} &V = U + \Omega + W = \iint F\,\mathrm{d}A \\ &\Rightarrow F = \frac{1}{2}[N_x(u_{0,x} + 0.5w_{0,x}^2 - \alpha_x \Delta T) - M_x w_{0,xx} + N_\theta[\frac{v_{0,\theta} + w_0}{R} + 0.5(\frac{w_{0,\theta}}{R})^2 - \alpha_\theta \Delta T] \\ &- M_{x\theta}(\frac{2w_{0,x\theta}}{R}) - M_\theta \frac{w_{0,\theta\theta}}{R^2} + N_{x\theta}(\frac{u_{0,\theta}}{R} + v_{0,x} + \frac{w_{0,x} w_{0,\theta}}{R}) + F_x \phi_{,x} + k_w w_0^2 + k_g(w_{0,x}^2 + \frac{w_{0,\theta}^2}{R^2})] - \tau h(u_{0,\theta} + v_{0,x}) \end{aligned} \tag{15}$$

In addition, equilibrium equations are specified as following, using Euler equations:

$$\begin{cases} RN_{x,x} + N_{x\theta,\theta} = 0 \\ RN_{x\theta,x} + N_{\theta,\theta} = 0 \\ RN_\theta + R^2 k_w w_0 - R^2 k_g w_{0,xx} - k_g w_{0,\theta\theta} - R^2 N_x w_{0,xx} \\ -2RN_{x\theta} w_{0,x\theta} - N_\theta w_{0,\theta\theta} - R^2 M_{x,xx} - 2RM_{x\theta,x\theta} - M_{\theta,\theta\theta} = 0 \\ F_{x,x} = 0 \end{cases} \tag{16}$$

2.6 The criterion of equilibrium in the vicinity

In order to achieve force and moment equations as well as stability equations, displacement values of u_0, v_0 and w_0 are superseded in formulas marked as (11) and (16), as below [4]:

$$\begin{aligned} u &\to u^0 + u^1 \\ v &\to v^0 + v^1 \\ w &\to w^0 + w^1 \end{aligned} \tag{17}$$

where (u^1, v^1, w^1) represents displacement arbitrary components, and (u^0, v^0, w^0) and (u, v, w) are two arbitrary sets which are close to stability. Thus, force and torque equations are derived as below:

$$\begin{cases} N_x^1 = A_{11}(u_{0,x}^1 + w_{0,x}^0 w_{0,x}^1) - A_{12} w_{0,xx}^1 + A_{13}(\frac{v_{0,\theta}^1 + w_0^1}{R} + \frac{w_{0,\theta}^0 w_{0,\theta}^1}{R^2}) - A_{14}\frac{w_{0,\theta\theta}^1}{R^2} \\ M_x^1 = A_{21}(u_{0,x}^1 + w_{0,x}^0 w_{0,x}^1) - A_{22} w_{0,xx}^1 + A_{23}(\frac{v_{0,\theta}^1 + w_0^1}{R} + \frac{w_{0,\theta}^0 w_{0,\theta}^1}{R^2}) - A_{24}\frac{w_{0,\theta\theta}^1}{R^2} \\ N_\theta^1 = A_{31}(u_{0,x}^1 + w_{0,x}^0 w_{0,x}^1) - A_{32} w_{0,xx}^1 + A_{33}(\frac{v_{0,\theta}^1 + w_0^1}{R} + \frac{w_{0,\theta}^0 w_{0,\theta}^1}{R^2}) - A_{34}\frac{w_{0,\theta\theta}^1}{R^2} \\ M_\theta^1 = A_{41}(u_{0,x}^1 + w_{0,x}^0 w_{0,x}^1) - A_{42} w_{0,xx}^1 + A_{43}(\frac{v_{0,\theta}^1 + w_0^1}{R} + \frac{w_{0,\theta}^0 w_{0,\theta}^1}{R^2}) - A_{44}\frac{w_{0,\theta\theta}^1}{R^2} \\ N_{x\theta}^1 = A_{55}(\frac{u_{0,\theta}^1}{R} + v_{0,x}^1 + \frac{w_{0,x}^0 w_{0,\theta}^1 + w_{0,x}^1 w_{0,\theta}^0 + w_{0,x}^1 w_{0,\theta}^1}{R}) - A_{56}(\frac{2w_{0,x\theta}^1}{R}) \\ M_{x\theta}^1 = A_{65}(\frac{u_{0,\theta}^1}{R} + v_{0,x}^1 + \frac{w_{0,x}^0 w_{0,\theta}^1 + w_{0,x}^1 w_{0,\theta}^0 + w_{0,x}^1 w_{0,\theta}^1}{R}) - A_{66}(\frac{2w_{0,x\theta}^1}{R}) \\ F_x^1 = A_{71}(u_{0,x}^1 + w_{0,x}^0 w_{0,x}^1) - A_{72} w_{0,xx}^1 + A_{73}(\frac{v_{0,\theta}^1 + w_0^1}{R} + \frac{w_{0,\theta}^0 w_{0,\theta}^1}{R^2}) - A_{74}\frac{w_{0,\theta\theta}^1}{R^2} \end{cases} \tag{18}$$

and stability equations are derived as follows [4]:

$$\begin{cases} RN^{1}_{x,x} + N^{1}_{x\theta,\theta} = 0 \\ RN^{1}_{x\theta,x} + N^{1}_{\theta,\theta} = 0 \\ RN^{1}_{\theta} + R^{2}k_{w}w^{1}_{0} - R^{2}k_{g}w^{1}_{0,xx} - k_{g}w^{1}_{0,\theta\theta} - R^{2}N^{0}_{x}w^{1}_{0,xx} \\ -R^{2}N^{1}_{x}w^{0}_{0,xx} - 2RN^{0}_{x\theta}w^{1}_{0,x\theta} - 2RN^{1}_{x\theta}w^{0}_{0,x\theta} - N^{0}_{\theta}w^{1}_{0,\theta\theta} \\ -N^{1}_{\theta}w^{0}_{0,\theta\theta} - R^{2}M^{1}_{x,xx} - 2RM^{1}_{x\theta,x\theta} - M^{1}_{\theta,\theta\theta} = 0 \\ F^{1}_{x,x} = 0 \end{cases} \tag{19}$$

2.7 Torsional buckling analysis

The effect of pre-buckling rotations in many cases is negligible. Moreover, it is possible to ignore the pre-buckling displacement in the circumferential direction, that's why in the intended equations $w^{0}_{0,x}, w^{0}_{0,\theta}$ equal zero. A cylinder under net torsional torque around its axial direction is defined as:

$$N^{0}_{x} = N^{0}_{\theta} = 0, N^{0}_{x\theta} = \frac{\tau}{h} \tag{20}$$

with substituting Eqs. (20) in Eqs. (19), stability equations are simplified as below:

$$\begin{cases} RN^{1}_{x,x} + N^{1}_{x\theta,\theta} = 0 \\ RN^{1}_{x\theta,x} + N^{1}_{\theta,\theta} = 0 \\ RN^{1}_{\theta} + R^{2}k_{w}w^{1}_{0} - R^{2}k_{g}w^{1}_{0,xx} - k_{g}w^{1}_{0,\theta\theta} - \\ 2RN^{0}_{x\theta}w^{1}_{0,x\theta} - R^{2}M^{1}_{x,xx} - 2RM^{1}_{x\theta,x\theta} - M^{1}_{\theta,\theta\theta} = 0 \\ F^{1}_{x,x} = 0 \end{cases} \tag{21}$$

Also with substituting Eqs. (18) into Eqs. (21), stability equations are obtained in terms of displacement:

$$\begin{cases} RC_{11}u^{1}_{0,xx} + C_{12}(v^{1}_{0,x\theta} + w^{1}_{0,x}) + \frac{C_{66}}{R}u^{1}_{0,\theta\theta} + C_{66}v^{1}_{0,x\theta} = 0 \\ C_{66}(u^{1}_{0,x\theta} + Rv^{1}_{0,xx}) + C_{12}u^{1}_{0,x\theta} + C_{22}(\frac{v^{1}_{0,\theta\theta} + w^{1}_{0,\theta}}{R}) = 0 \\ C_{12}Rhu^{1}_{0,x} + C_{22}h(v^{1}_{0,\theta} + w^{1}_{0}) - \frac{2R\tau}{h}w^{1}_{0,x\theta} + \frac{1}{12}R^{2}C_{11}hw^{1}_{0,xxxx} \\ +(\frac{C_{12}h + 2C_{66}h}{6}) + \frac{C_{22}h}{12R^{2}}w^{1}_{0,\theta\theta\theta} + R^{2}k_{w}w^{1}_{0} - R^{2}k_{g}w^{1}_{0,xx} - k_{g}w^{1}_{0,\theta\theta} = 0 \\ e_{31}u^{1}_{0,xx} + e_{32}(\frac{v^{1}0,x\theta + w^{1}_{0,x}}{R}) = 0 \end{cases} \tag{22}$$

Hence, assumed isotropic, the matrix will be verified through equations in[30]. As depicted below, the deformation of the buckling in cylindrical shells under torsional loads is expressed as a function of axial and circumferential waves.

$$\begin{cases} u_0^1 = \sum\sum U_{mn} \cos(\bar{m}x - n\theta) \\ v_0^1 = \sum\sum V_{mn} \cos(\bar{m}x - n\theta) \\ w_0^1 = \sum\sum W_{mn} \sin(\bar{m}x - n\theta) \end{cases} \tag{23}$$

$$\bar{m} = m\pi/L \tag{24}$$

where m and n represent the number of half-waves in the axial direction and the number of full waves in the circumferential direction, respectively. So, substitution of Eqs. (23) into Eqs. (22) derives the following matrix:

$$\begin{bmatrix} L_{11} & L_{12} & L_{13} \\ L_{21} & L_{22} & L_{23} \\ L_{31} & L_{32} & L_{33} \end{bmatrix} \begin{Bmatrix} U_{mn} \\ V_{mn} \\ W_{mn} \end{Bmatrix} = \begin{Bmatrix} 0 \\ 0 \\ 0 \end{Bmatrix} \tag{25}$$

where coefficients $L_{ij}\,(i, j = 1,2,3)$ are given as below:

$$L_{11} = -(R^2 C_{11}\bar{m}^2 + \frac{e_{31}}{e_{32}} R^2 C_{12}\bar{m}^2 + C_{66}n^2) \qquad L_{12} = -RC_{66}\bar{m}n \qquad L_{13} = 0$$
$$L_{21} = R\bar{m}n(C_{12} + C_{66}) \qquad L_{22} = -R^2\bar{m}^2 - C_{22}n^2 \qquad L_{23} = -C_{22}n$$
$$L_{31} = -12R^3h^2C_{12}\bar{m}^2 - \frac{12R^3h^2C_{22}e_{31}}{e_{32}}\bar{m}^2 \qquad L_{32} = 0 \qquad \bar{m} = \frac{m\pi R}{L}$$
$$L_{33} = -24R^3\bar{m}^2n\tau + R^4C_{11}h^2\bar{m}^5 + 2R^2h^2C_{12}\bar{m}^3n^2 + 4R^2h^2\bar{m}^3n^2C_{66}$$
$$+C_{22}h^2\bar{m}n^4 + 12hR^4k_w\bar{m} + 12hR^4k_g\bar{m}^3 + 12hR^2k_g\bar{m}n^2$$

In order for the equations system (24) to have a unique answer, it is required the determinant of the coefficient matrix equals zero. Consequently, the critical torsional load is specified as:

$$\tau = \frac{Q_1}{Q_2} \tag{26}$$

$$Q_2 = 24e_{31}R^7C_{12}\bar{m}^5n - 24e_{32}R^3C_{22}C_{66}\bar{m}n^5 + 24e_{31}R^5C_{12}C_{22}\bar{m}^3n^3 + 24e_{32}R^5C_{11}C_{22}\bar{m}^3n^3$$
$$+24e_{32}R^5C_{12}C_{66}\bar{m}^2n^4 + 24e_{32}R^5C_{66}^2\bar{m}^2n^4 + 24e_{32}R^7C_{11}\bar{m}^5n + 24e_{32}R^5C_{66}\bar{m}^3n^2 \tag{27}$$

and

$$Q_1 = e_{32}R^8C_{11}^2h^2\bar{m}^8 + 2e_{32}R^6h^2C_{11}C_{12}\bar{m}^6n^2 + e_{32}R^4h^2C_{11}C_{22}\bar{m}^4n^4 + 12e_{32}R^8hC_{11}k_w\bar{m}^4$$
$$+12e_{32}R^8hC_{11}k_g\bar{m}^6 + 12e_{32}R^6hC_{11}k_g\bar{m}^4n^2 + e_{31}R^8h^2C_{11}C_{12}\bar{m}^8 + 2e_{31}R^6h^2C_{12}^2\bar{m}^6n^2$$
$$+4e_{31}R^6h^2C_{12}C_{66}\bar{m}^6n^2 + e_{31}R^4h^2C_{12}C_{22}\bar{m}^4n^4 + 12e_{31}R^8hC_{12}k_w\bar{m}^4 + 12e_{31}R^8hC_{12}k_g\bar{m}^6$$
$$+12e_{31}R^6hC_{12}k_g\bar{m}^4n^2 + 5e_{32}R^6h^2C_{11}C_{66}\bar{m}^6n^2 + 2e_{32}R^4h^2C_{12}C_{66}\bar{m}^4n^4 + 4e_{32}R^4h^2C_{66}^2\bar{m}^4n^4 \tag{28}$$

$$
\begin{aligned}
&+e_{32}R^2h^2C_{22}C_{66}\bar{m}^2n^6+12e_{32}R^6hC_{66}k_w\bar{m}^2n^2+12e_{32}R^6hC_{66}k_g\bar{m}^4n^2+12e_{32}R^4hC_{66}k_g\bar{m}^2n^4\\
&+e_{32}R^6h^2C_{11}^2C_{22}\bar{m}^6n^2+2e_{32}R^4h^2C_{11}C_{12}C_{22}\bar{m}^4n^4+5e_{32}R^4h^2C_{11}C_{22}C_{66}\bar{m}^4n^4+e_{32}R^2h^2C_{11}C_{22}^2\bar{m}^2n^6\\
&+12e_{32}R^6hC_{11}C_{22}k_w\bar{m}^2n^2+12e_{32}R^6hC_{11}C_{22}k_g\bar{m}^4n^2+12e_{32}R^4hC_{11}C_{22}k_g\bar{m}^2n^4\\
&+e_{31}R^6h^2C_{11}C_{12}C_{22}\bar{m}^6n^2+2e_{31}R^4h^2C_{12}^2C_{22}\bar{m}^4n^4+4e_{31}R^4h^2C_{12}C_{22}C_{66}\bar{m}^4n^4+2e_{31}R^4h^2C_{12}^2C_{22}\bar{m}^4n_4\\
&+4e_{31}R^4h^2C_{12}C_{22}C_{66}\bar{m}^4n^4+e_{31}R^2h^2C_{12}C_{22}^2\bar{m}^2n^6+12e_{31}R^6hC_{12}C_{22}k_w\bar{m}^2n^2+12e_{31}R^6hC_{12}C_{22}k_g\bar{m}^4n^2\\
&+12e_{31}R^4hC_{12}C_{22}k_g\bar{m}^2n^4+2e_{32}R^2h^2C_{12}C_{22}C_{66}\bar{m}^2n^6+4e_{32}R^2h^2C_{22}C_{66}^2\bar{m}^2n^6+e_{32}h^2C_{22}^2C_{66}n^8\\
&+12e_{32}R^4hC_{22}C_{66}k_wn^4+12e_{32}R^4hC_{22}C_{66}k_g\bar{m}^2n^4+12e_{32}hR^2C_{22}C_{66}k_gn^6+e_{32}R^6h^2C_{11}C_{12}C_{66}\bar{m}^5n^3\\
&+2e_{32}R^4h^2C_{12}^2C_{66}\bar{m}^3n^5+6e_{32}h^2R^4C_{12}C_{66}^2\bar{m}^3n^6+e_{32}R^2h^2C_{12}C_{22}C_{66}\bar{m}n^7+12e_{32}R^6hC_{12}C_{66}k_w\bar{m}n^3\\
&+12e_{32}hR^6C_{12}C_{66}k_g\bar{m}^3n^3+12e_{32}R^4hC_{12}C_{66}k_g\bar{m}n^5+e_{32}R^6h^2C_{11}C_{66}^2\bar{m}^3n^3+4e_{32}h^2R^4C_{66}^3\bar{m}^3n^5\\
&+e_{32}R^2h^2C_{22}C_{66}^2\bar{m}n^7+12e_{32}R^6hC_{66}^2\bar{m}n^3+12e_{32}hR^6C_{66}^2k_g\bar{m}^3n^3+12e_{32}R^4hC_{66}^2k_g\bar{m}n^5\\
&-12e_{32}R^4h^2C_{12}C_{22}C_{66}\bar{m}n^3-12e_{31}h^2R^4C_{22}^2C_{66}\bar{m}n^3
\end{aligned}
\tag{28}
$$

3 RESULTS AND DISCUSSION

Mechanical, electrical, and thermal characteristics of PVDF matrix and DWBNNTs reinforce are presented in Table 1; and the amounts are calculated for a shell with features of $L = 6000\ mm$, $R = 60\ mm$, and $h = 6\ mm$ [28].

Table 1
Mechanical, electrical and thermal properties of PVDF and DWBNNTs.

PVDF		DWBNNTs
$C_{11}=238.24(Gpa)$	$e_{11}=-0.135(C/m^2)$	$E=1.8(Tpa)$
$C_{12}=3.98(Gpa)$	$e_{12}=-0.145(C/m^2)$	
$C_{13}=2.19(Gpa)$	$e_{31}=-0.13(C/m^2)$	$\nu=0.34$
$C_{22}=23.6(Gpa)$	$e_{32}=-0.145(C/m^2)$	$e_{11}=0.95(C/m^2)$
$C_{23}=1.92(Gpa)$	$e_{24}=-0.145(C/m^2)$	$\alpha_x=1.2\times10^{-6}(1/K)$
$C_{33}=10.64(Gpa)$	$e_{15}=-0.009(C/m^2)$	$\alpha_\theta=0.6\times10^{-6}(1/K)$
$C_{44}=2.15(Gpa)$	$\in_{11}=\in_{22}=\in_{33}=1.1068\times10^{-8}(F/m)$	$k_x=4\times10^4$
$C_{55}=4.4(Gpa)$	$\alpha_x=\alpha_\theta=7.1\times10^{-5}(1/K)$	$k_g=4\times10^{-6}$
$C_{66}=6.43(Gpa)$	$\rho=0.2$	

In order to verify the equations of critical torsional load, it was assumed that the whole shell to be isotropic with the constants of $\nu = 0.3$ and $E = 380\ GPa$. The achieved results are represented in Table 2 [9]:

Table 2
Verification of critical torsional load (*GPa*) for a homogeneous shell with $\nu = 0.3$, $E = 380\ GPa$.

L/R	*R/h*	*m*	*n*	REF [10]	Present
10	10	1	2	4773.523	4827.375
10	50	1	2	361.334	361.423
10	100	1	3	176.814	176.562
10	500	1	4	20.036	20.036
40	10	2	1	1860.974	1860.259
40	50	1	1	180.624	180.631
40	100	1	1	113.352	113.351
40	500	1	2	9.978	9.978
100	10	4	1	1789.934	1794.258
100	50	2	1	158.390	158.426
100	100	1	1	61.372	61.372
100	500	1	1	8.097	8.099

As shown in Table 2, the effect of various parameters on critical torsional load for a homogenous shell with specifications of v = 0.3 and E = 380 *GPa* has been investigated. Results of this investigation has been compared with the results yielded byNajafizadeh and Khazaeinejad [9], for various amounts of m and n as well as for different ratios of L/R i.e. 10, 40, and 100, and for different ratios of L/R which are 10, 50, 100, and 500. The comparison demonstrates for higher ratios of R/h, that is 50, 100, and 500, regardless of the ratio of L/R, alterations are slight with the highest amount of 0.25 *GPa*. Whereas, for lower ratios of R/h as 10 the changes are noticeable, with the highest amount of 53.85 *GPa* increase in the produced results which is equivalent to 1.1 percent where L/R, n, and m are 10, 2, and 1, respectively. In addition, this change is 4.3 *GPa* equivalent to 0.2 percent increase in the generated results in this research for L/R = 100, n = 1, and m = 4. Considering the alteration are insignificant and negligible, the results revealed in this paper are verified through comparison with the results derived by byNajafizadeh and Khazaeinejad [9].

3.1 Determination of critical m and n

Generating solutions, through MATLAB package, for the developed equations, Table 3; presents the critical torsional buckling load, τ_{cr}, for various axial half-wave numbers, m, and circumferential wave numbers, n, at L/R = 100 and R/h = 10. The minimum amount of critical torsional load occurred at m = 24 and n = 1, with the magnitude of 0.218 *GPa*. The circumferential wave number directly affected the critical load (Fig. 3); hence with the increase of this number the load increased, such that with n=20 and m=20, the load equaled $2\times10^{12}\,Pa$. The impact of various axial half-wave numbers and circumferential wave numbers at L/R = 100 and R/h = 10 on τ_{cr} is depicted in Fig. 4.

Table 3
Critical torsional loads for PVDF reinforced with DWBNNTs for L/R = 100 and R/h = 10.

L/R	R/h	m	n	Critical torsional buckling (GPa) $\times10^5$
100	10	1	1	5.124
100	10	1	2	2.5
100	10	1	3	1.619
100	10	1	4	1.176
100	10	1	5	0.914
100	10	1	24	0.218
100	10	2	1	41.34
100	10	3	1	139.5
100	10	4	1	330.8
100	10	5	1	646

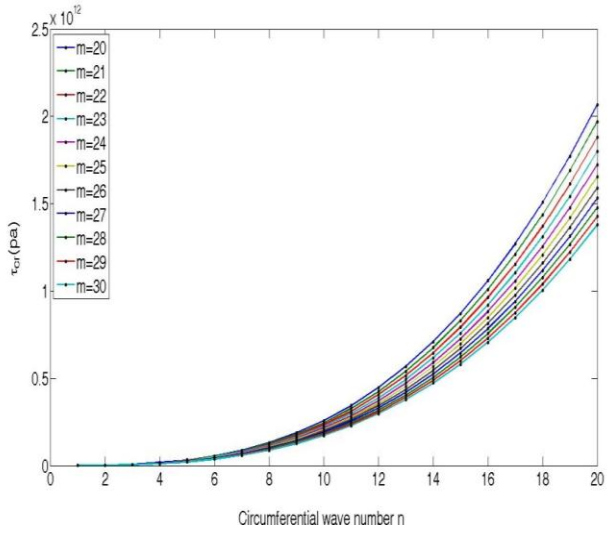

Fig.3
Critical torsional load as a function of n for L/R = 100 and R/h = 10.

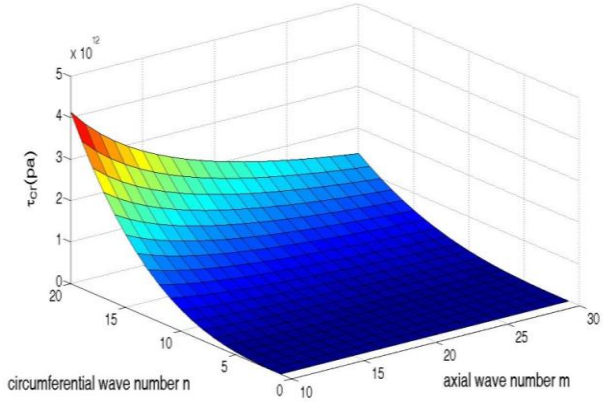

Fig.4
Critical torsional load as a function of *n* and *m* for *L/R* = 100 and *R/h* = 10.

3.2 Effect of the length-to-radius ratio on the critical torsional load

Fig.5 demonstrates the critical torsional load as a function of length-to-radius. As shown, the critical torsional load increased with the increase of the *L/R* ratio and having a constant *R/h* ratio while *m*=*n*=1. Interestingly, the increase takes place nearly linearly. The quantitative changes of the critical torsional load in terms of length to radius are presented in Table 4.

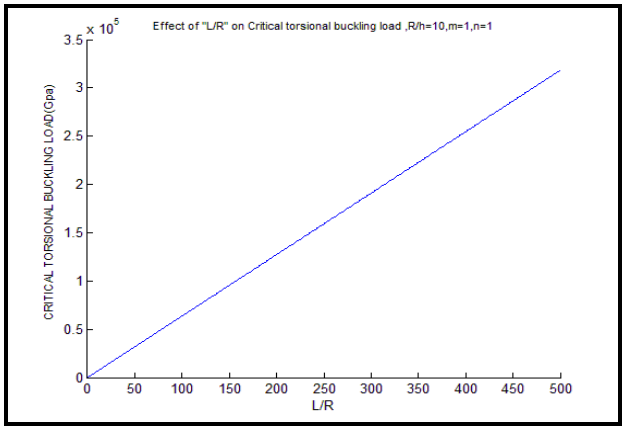

Fig.5
Critical torsional load in terms of length to radius (*L/R*).

Table 4
The critical torsional load as a function of *L/R* for *m* = *n* = 1 and *R/h* = 10.

L/R	*R/h*	*m*	*n*	Critical torsional buckling (*GPa*) $\times 10^5$
50	10	1	1	0.25
100	10	1	1	0.51
200	10	1	1	1.03
300	10	1	1	1.55
400	10	1	1	2.07
500	10	1	1	2.58

3.3 Effect of the radius-to-thickness ratio on the critical torsional load

As demonstrated in Fig.6, unlike the *L/R* ratio, the critical torsional load decreases when the ratio of radius to shell thickness increases. The critical load reduces drastically by the increase of the *R/h* ratio up to 20; then the critical load reaches a steady state with the increase of *R/h* ratio. The experiment took place when *L/R* = 100 and *m*=*n*=1. The quantitative changes of the critical torsional load as a function of the radius-to-the shell thickness ratio are also represented in Table 5.

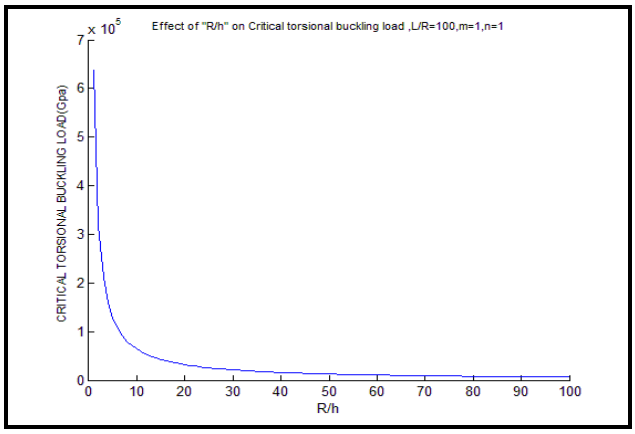

Fig.6
Critical torsional load as a function of radius to thickness (*R/h*).

Table 5
The critical torsional load as a function of *R/h* for $m = n = 1$ and $L/R = 100$.

L/R	*R/h*	*m*	*n*	Critical torsional buckling (*GPa*) $\times 10^5$
100	10	1	1	5.124
100	30	1	1	0.569
100	50	1	1	0.205
100	80	1	1	0.008
100	100	1	1	0.005

3.4 Effect of nanotubes volume fraction on the critical torsional load

The critical torsional load as a function of nanotubes volume fraction is demonstrated in Fig.7. The critical torsional load increased by the increase of volume fraction of the nanotubes. As demonstrated for the nanotube volume fraction increase between 0.2 to 0.7, the critical load increases approximately linearly; whereas for higher volume fractions the increase of the critical load behaves non-linearly and at a higher rate.

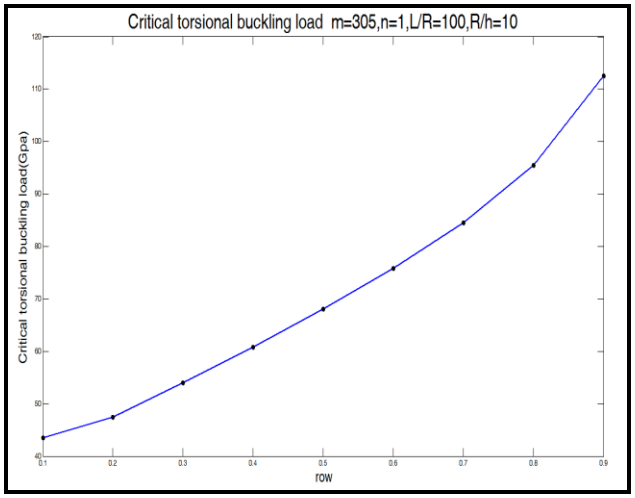

Fig.7
Critical torsional load as a function of nanotubes volume fraction.

4 CONCLUSION

In this study, equilibrium and stability equations of a piezoelectric cylindrical shell, reinforced with DWBNNTs were obtained. Then, non-linear torsional buckling under a combination of electro-thermo-mechanical loadings was investigated in elastic medium including Winkler and Pasternak foundation. The torsional buckling load for the

piezoelectric cylindrical shell reinforced with DWBNNTs under the combination of electro-thermo-mechanical loadings was computed to be critical at $m = 24$ and $n = 1$. Additionally, the critical torsional buckling load for the reinforced piezoelectric cylindrical shell under the combination of electro-thermo-mechanical loadings, in the elastic foundation, increased by the increase of the length-to-radius ratio. This load, however, decreased with the increase in the radius-to-shell thickness ratio. Finally, the increase of the volume fraction of nanotubes also directed affect the critical torsional buckling loads. That is, an increase in the amount of reinforcements in the matrix resulted in an increase of the critical torsional buckling loads.

Future work of this paper would be the investigation of boundary conditions on the critical torsional buckling loads. Additionally, in this paper the classical shell method is used which has the limitations of being applicable on composites with low bucklings, and neglecting the strain energy; hence, we are interested in the comparison of results of this work with other types of reinforcements like CNTs nanotubes; and to generate solutions for the developed equations through the first order and higher order shear deformation theory in order to compare the results with the results presented in this work.

REFERENCES

[1] Brockmann T.H., 2009, *Theory of Adaptive Fiber Composites: From Piezoelectric Material Behavior to Dynamics of Rotating Structures*, Springer Science & Business Media.

[2] Uzun B., Numanoglu H., Civalek O., 2018, Free vibration analysis of BNNT with different cross-Sections via nonlocal FEM, *Journal of Computational Applied Mechanics* **49**(2): 252-260.

[3] Sofiyev A., 2010, Buckling analysis of FGM circular shells under combined loads and resting on the Pasternak type elastic foundation, *Mechanics Research Communications* **37**(6): 539-544.

[4] Miraliyari O., Najafizadeh M.M., Rahmani A.R., Momeni Hezaveh A., 2011, Thermal and mechanical buckling of short and long functionally graded cylindrical shells using third order shear deformation theory, *World Academy of Science, Engineering and Technology International Journal of Mechanical and Mechatronics Engineering* **5**(2): 518-522.

[5] Bagherizadeh E., Kiani Y., Eslami M., 2011, Mechanical buckling of functionally graded material cylindrical shells surrounded by Pasternak elastic foundation, *Composite Structures* **93**(11): 3063-3071.

[6] Najafizadeh M.M., Hasani A., Khazaeinejad P., 2009, Mechanical stability of functionally graded stiffened cylindrical shells, *Applied Mathematical Modelling* **33**(2): 1151-1157.

[7] Sheng G., Wang X., 2010, Thermoelastic vibration and buckling analysis of functionally graded piezoelectric cylindrical shells, *Applied Mathematical Modelling* **34**(9): 2630-2643.

[8] Shen H.-S., Yang J., Kitipornchai S., 2010, Postbuckling of internal pressure loaded FGM cylindrical shells surrounded by an elastic medium, *European Journal of Mechanics-A/Solids* **29**(3): 448-460.

[9] Najafizadeh M.M., Khazaeinejad P., 2011, Buckling of nonhomogeneous cylindrical shells under torsion using first order shear deformation theory, *National Conference on New Technologies in Mechanical Engineering*, Iran.

[10] Hassani H.S., 2010, Transient heat transfer analysis of hydraulic system for JD 955 harvester combine by finite element method, *Journal of Food, Agriculture & Environment* **8**(2): 382-385.

[11] Arani A.G., 2012, Electro-thermo-mechanical buckling of DWBNNTs embedded in bundle of CNTs using nonlocal piezoelasticity cylindrical shell theory, *Composites Part B: Engineering* **43**(2): 195-203.

[12] Shadmehri F., Hoa S., Hojjati M., 2012, Buckling of conical composite shells, *Composite Structures* **94**(2): 787-792.

[13] Arani A.G., 2011, Semi-analytical solution of time-dependent electro-thermo-mechanical creep for radially polarized piezoelectric cylinder, *Computers & Structures* **89**(15): 1494-1502.

[14] Khazaeinejad P., 2010, On the buckling of functionally graded cylindrical shells under combined external pressure and axial compression, *Journal of Pressure Vessel Technology* **132**(6): 064501.

[15] Zargaripoor A., 2018, Free vibration analysis of nanoplates made of functionally graded materials based on nonlocal elasticity theory using finite element method, *Journal of Computational Applied Mechanics* **49**(1): 86-101.

[16] Moradi A., 2018, Magneto-thermo mechanical vibration analysis of FG nanoplate embedded on Visco Pasternak foundation, *Journal of Computational Applied Mechanics* **49**(2): 395-407.

[17] Mohammadi M., 2013, Temperature effect on vibration analysis of annular graphene sheet embedded on visco-Pasternak foundation, *Journal of Solid Mechanics* **5**(3): 305-323.

[18] Goodarzi M., 2014, Investigation of the effect of pre-stressed on vibration frequency of rectangular nanoplate based on a visco-Pasternak foundation, *Journal of Solid Mechanics* **6**(1): 98-121.

[19] Shen H.-S., Zhang C.-L., 2010, Torsional buckling and postbuckling of double-walled carbon nanotubes by nonlocal shear deformable shell model, *Composite Structures* **92**(5): 1073-1084.

[20] Mantari J., Oktem A., Soares C.G., 2012, A new higher order shear deformation theory for sandwich and composite laminated plates, *Composites Part B: Engineering* **43**(3): 1489-1499.

[21] Hassani H.S., 2011, Fatigue analysis of hydraulic pump gears of JD 1165 harvester combine through finite element method, *Trends in Applied Sciences Research* **6**(2): 174.

[22] Arani A.G., Kolahchi R., Barzoki A.M., 2011, Effect of material in-homogeneity on electro-thermo-mechanical behaviors of functionally graded piezoelectric rotating shaft, *Applied Mathematical Modelling* **35**(6): 2771-2789.
[23] Arani A.G., 2013, Electro-thermo-torsional buckling of an embedded armchair DWBNNT using nonlocal shear deformable shell model, *Composites Part B: Engineering* **51**: 291-299.
[24] Arani A.G., 2012, Electro-thermo-mechanical nonlinear nonlocal vibration and instability of embedded micro-tube reinforced by BNNT, conveying fluid, *Physica E: Low-Dimensional Systems and Nanostructures* **45**: 109-121.
[25] Ansari R., Rouhi S., Ahmadi M., 2018, On the thermal conductivity of carbon nanotube/polypropylene nanocomposites by finite element method*, Journal of Computational Applied Mechanics* **49**(1): 70-85.
[26] Barzoki A.M., 2012, Electro-thermo-mechanical torsional buckling of a piezoelectric polymeric cylindrical shell reinforced by DWBNNTs with an elastic core, *Applied Mathematical Modelling* **36**(7): 2983-2995.
[27] Kargarnovin M., Shahsanami M., 2012, Buckling analysis of a composite cylindrical shell with fiber's material properties changing lengthwise using first-order shear deformation theory, *International Conference on Mechanical, Automotive and Materials Engineering*.
[28] Barzoki A.M., 2013, Nonlinear buckling response of embedded piezoelectric cylindrical shell reinforced with BNNT under electro–thermo-mechanical loadings using HDQM, *Composites Part B: Engineering* **44**(1): 722-727.
[29] Tan P., Tong L., 2001, Micro-electromechanics models for piezoelectric-fiber-reinforced composite materials*, Composites Science and Technology* **61**(5): 759-769.
[30] Brush D.O., Almroth O., 1975, *Buckling of Bars, Plates and Shells,* New York, McGraw Hill.